MULTISCALE MODEL. SIMUL.
Vol. 13, No. 2, pp. 472–490



# HOMOGENIZATION OF HIGH-CONTRAST BRINKMAN FLOWS*

DONALD L. BROWN†, YALCHIN EFENDIEV‡, GUANGLIAN LI§, AND VIKTORIA SAVATOROVA¶

**Abstract.** Modeling porous flow in complex media is a challenging problem. Not only is the problem inherently multiscale but, due to high contrast in permeability values, flow velocities may differ greatly throughout the medium. To avoid complicated interface conditions, the Brinkman model is often used for such flows [O. Iliev, R. Lazarov, and J. Willems, *Multiscale Model. Simul.*, 9 (2011), pp. 1350–1372]. Instead of permeability variations and contrast being contained in the geometric media structure, this information is contained in a highly varying and high-contrast coefficient. In this work, we present two main contributions. First, we develop a novel homogenization procedure for the high-contrast Brinkman equations by constructing correctors and carefully estimating the residuals. Understanding the relationship between scales and contrast values is critical to obtaining useful estimates. Therefore, standard convergence-based homogenization techniques [G. A. Chechkin, A. L. Piatniski, and A. S. Shamev, *Homogenization: Methods and Applications*, Transl. Math. Monogr. 234, American Mathematical Society, Providence, RI, 2007, G. Allaire, *SIAM J. Math. Anal.*, 23 (1992), pp. 1482–1518], although a powerful tool, are not applicable here. Our second point is that the Brinkman equations, in certain scaling regimes, are invariant under homogenization. Unlike in the case of Stokes-to-Darcy homogenization [D. Brown, P. Popov, and Y. Efendiev, *GEM Int. J. Geomath.*, 2 (2011), pp. 281–305, E. Marusic-Paloka and A. Mikelic, *Boll. Un. Mat. Ital. A* (7), 10 (1996), pp. 661–671], the results presented here under certain velocity regimes yield a Brinkman-to-Brinkman upscaling that allows using a single software platform to compute on both microscales and macroscales. In this paper, we discuss the homogenized Brinkman equations. We derive auxiliary cell problems to build correctors and calculate effective coefficients for certain velocity regimes. Due to the boundary effects, we construct a boundary correction for the correctors similar to [O. A. Oleinik, G. A. Iosif'yan, and A. S. Shamaev, *Mathematical Problems in Elasticity and Homogenization*, Elsevier, Amsterdam, 1992]. Using residuals, we estimate for both pore-scales, $\varepsilon$, and contrast values, $\delta$, to obtain our corrector estimates. We then implement the homogenization procedure numerically on two media, the first being Stokes flow in fractures with Darcy-like inclusions and the second being Darcy-like flow with Stokesian vuggs. In these examples, we observe our theoretical convergence rates for both pore-scales and contrast values.

**Key words.** homogenization, Brinkman flow, porous media, high contrast

**AMS subject classifications.** 35B27, 76S05, 76M10

**DOI.** 10.1137/130908294

## 1. Introduction.

Understanding flow in porous media is critical, as it has wide ranging applications in subsurface modeling and filtration devices for industrial appli-

*Received by the editors February 1, 2013; accepted for publication (in revised form) January 23, 2015; published electronically April 16, 2015.
http://www.siam.org/journals/mms/13-2/90829.html

†Institute for Numerical Simulation, University of Bonn, Bonn 53115, Germany (brown@ins.uni-bonn.de).

‡Center for Numerical Porous Media (NumPor), King Abdullah University of Science and Technology (KAUST), Thuwal 23955-6900, Kingdom of Saudi Arabia. Current address: Department of Mathematics & Institute for Scientific Computation (ISC), Texas A&M University, College Station, TX 77843 (efendiev@math.tamu.edu). This author's research was partially supported by the U.S. Department of Energy Office of Science, Office of Advanced Scientific Computing Research, Applied Mathematics program under award DE-FG02-13ER26165, by DOE 489141, and by the DoD Army ARO Project.

§Department of Mathematics & Institute for Scientific Computation (ISC), Texas A&M University, College Station, TX 77843 (lotusli0707@gmail.com).

¶Physics Department, N6 NRNU MEPhI, Moscow 115409, Russia (vsavatorova@gmail.com). This author's research was partially supported by Federal Target Program "Research and development on priority directions of scientific-technological complex of Russia for 2007–2013 (11.519.11.6036)."

cations. Due to complex physics and heterogeneous geometry, modeling of such media is often challenging. The primary physical description for porous media flow relies on Darcy's law [5]. The Darcy equation is the workhorse equation for many industrial applications. However, for many applications this is insufficient. For example, in the case of vuggy carbonate reservoirs or low porosity filtration devices, the Darcy equation is not sufficient to describe the essential physics (cf. [9, 12]). To account for these varying flow regions in porous media, the Brinkman equation is used.

By adding a viscous term to the mixed formulation of the Darcy system, we obtain the Brinkman equation that can account for fast flow regions such as channels or vuggs. From a converse viewpoint, by adding a drag term to the Stokes flow equations, we account for flow through portions of the media with lower permeability. The Brinkman model has the advantage of a single equation formulation over the Stokes–Darcy system with complicated interface conditions [2]. Information of high and low flow regions in the geometry are completely contained in the coefficients related to permeability. Porous media is inherently multiscale, making simulating the fine-scale equations computationally expensive. Often, such a description is undesirable and an effective or homogenized description is preferred. In addition to the Brinkman equations depending on multiple scales, the coefficients must contain information about high and low flow regions. Thus, the coefficients also have a high contrast.

Understanding the relationship between the spatial scales and contrast is crucial to obtaining a macroscopic flow description. Due to the problem's high-contrast nature, standard weak-convergence-based homogenization methods [4, 1] are insufficient in understanding the scale-contrast relationship. To this end, we employ two-scale asymptotic expansions [13] and build and estimate correctors to the fine-scale solution to obtain and prove the homogenization (cf. [3, 10]). The main difficulty is understanding which contrast values will lead to legitimate corrector estimates that will converge in the homogenization limit.

Once these values are established, we are able to obtain a Brinkman-to-Brinkman homogenization result for certain velocity regimes. More precisely, the high-contrast fine-scale Brinkman equation, once homogenized, results in a Brinkman-type macroscopic equation. A similar result occurs when homogenizing Darcy equations and, more generally, elliptic equations [1]. This equation invariance is not guaranteed in the homogenization limit. For example, in the pore-scale modeling case, Stokes equations being in a solid skeleton is an often utilized fine-scale model. The homogenization process in this setting yields the Darcy equations [15]. The macroscopic equation is of a fundamentally different structure. There are computational advantages of having a unified fine-scale/coarse-scale framework. Assuming the fine- and coarse-scale equations parameters do not significantly differ, that is, do not degenerate to pure Stokes for example, the system may be solved using the same software platforms. Developing new discretization methods, new solvers, and associated preconditioners for two structurally different equations is not computationally efficient.

In this paper, we derive correctors to the fine-scale Brinkman equation via two-scale expansion techniques. The constructed correctors do not satisfy global boundary conditions, and a boundary correction must be added as in [17]. We assume the characteristic scale size is $\varepsilon$ and the parameter associated with the contrast value is $\delta$. We estimate the homogenization convergence rate in terms of $\varepsilon$ and $\delta$.

To corroborate the theory and to gain more insight, we perform several two-dimensional numerical examples. We implement quadratic velocity and constant pressure $\mathbb{P}_2^2/\mathbb{P}_0$ finite elements to build first-order correctors, compute the effective Brinkman coefficient, and solve both the fine-scale and homogenized Brinkman equa-

tions. Numerical results are presented to show that the proposed correctors converge in $\varepsilon$ and the rates are consistent with our analysis. The implementation is applied to two periodic high-contrast coefficients. The two examples are of a periodic square inclusion. In two dimensions, such a geometry has a connected region and a disconnected region. We suppose the first example is the Stokes flow regime in the connected component and Darcy contrast values in the square inclusion. The second example is the Darcy regime in the connected component with Stokes flow in the square vuggs. We observe that the correctors perform well when $\delta$ is not very small compared with $\varepsilon$. More precisely, this occurs when contrast is not very large with respect to the small scales.

This paper is organized as follows. First, we present the preliminaries and background of the fine-scale Brinkman equations with high-contrast coefficients, and then we construct the correctors for velocity and pressure based on the cell equation and homogenized equation and present the main result of our paper in section 2. In section 3, we exhibit the numerical results with various $\delta$ and $\varepsilon$ for different high-contrast media. Due to the boundary layers, in section 4, we adapt the correctors constructed in section 2 by adding a boundary correction. Then, we present a proof for our main result. In section 5, we summarize the results of the paper. In the appendix, we present the auxiliary estimates needed for section 4.

**2. Homogenization of high-contrast Brinkman equations.** In this section, we begin by introducing the fine-scale Brinkman equations with high-contrast coefficients. We introduce the notion of periodic media and assumptions on the contrast values. The homogenized Brinkman system is presented. To prove the homogenization, we build correctors from cell problems. Finally, we state our main convergence theorem and discuss the ramifications of the results by using an illustrative example.

**2.1. Preliminaries.** We begin by formulating the problem in a more mathematical description. First, let $\Omega \subset \mathbb{R}^d$ be a sufficiently smooth bounded domain. We suppose that the characteristic pore size is $\varepsilon$ and the value related to the contrast is $\delta$. We have the fine-scale Brinkman equations of the form

$$\nabla p_\varepsilon(x) - \Delta u_\varepsilon(x) + \alpha_\varepsilon^\delta(x) u_\varepsilon(x) = f(x) \text{ in } \Omega, \tag{1a}$$

$$\operatorname{div}(u_\varepsilon(x)) = 0 \text{ in } \Omega, \quad u_\varepsilon(x) = 0 \text{ on } \partial\Omega. \tag{1b}$$

Here, $u_\varepsilon$ is the velocity, $p_\varepsilon$ is the pressure, and $\alpha_\varepsilon^\delta$ is a symmetric and positive definite Brinkman tensor. Moreover, we suppose $\alpha_\varepsilon^\delta$ is periodic with respect to the fast (cell) variable $y = x/\varepsilon$ and all of the spatial scaling is contained in this variable. More precisely, we may write $\alpha_\varepsilon^\delta(x) = \alpha^\delta(\frac{x}{\varepsilon})$. We relate the Brinkman coefficient to the permeability, $K$, via the inverse relation $\alpha = K^{-1}$. If permeability is high, the resistive term is diminished and the medium is in the Stokesian regime. Conversely, if $K$ is small, then the viscous term is diminished and the Darcy resistive term dominates.

To model media in which there are both high flow and low flow regions, we will assume $\alpha_\varepsilon^\delta$ can have very large variations. More precisely, we assume there exist a $\delta > 0$ and $\eta_1, \eta_2$ such that

$$C_1 \delta^{\eta_1} \leq \left| \alpha^\delta \left( \frac{x}{\varepsilon} \right) \right| \leq C_2 \delta^{\eta_2} \tag{2}$$

for all $x \in \Omega$. The contrast of the media, $\kappa = (\delta^{\eta_2}/\delta^{\eta_1})$, can be very large. The contrast parameter $\delta$ may or may not be connected to the characteristic scale size $\varepsilon$. In this way, we can enforce Darcy and Stokes flow regions of flow depending on the contrast value $\alpha$. For clarity's sake, we will drop the $\delta$ from $\alpha$ notation.

Since $\alpha$ is periodic, the domain can be decomposed into periodic unit cell translations as

$$\Omega = \bigcup_{j=1}^{N_\varepsilon} \varepsilon\,(Y + k_j)\,,$$

where $Y$ is the unit cell, $N_\varepsilon = O(1/\varepsilon^d)$ is the number of cells, and $k_j \in \mathbb{Z}^d$. With the intent of obtaining a homogenized fine-scale model (1) description, we solve cell problems on the unit cell domain $Y$. From these quantities we will obtain an averaged Brinkman coefficient $\alpha^*$. The effective coefficient may still depend on $\delta$, but not the scale $\varepsilon$, and will satisfy the bounds (2).

After the averaging procedure, we arrive at the homogenized Brinkman equations

$$\nabla \bar{p} - \Delta \bar{u} + \alpha^* \bar{u} = f \text{ in } \Omega, \tag{3a}$$

$$\operatorname{div}(\bar{u}) = 0 \text{ in } \Omega, \quad \bar{u} = 0 \text{ on } \partial\Omega. \tag{3b}$$

The scaling of $\alpha^*$ will be of particular importance in our numerical results. For large values of $\alpha^*$, the homogenized equations will enter the Darcy regime; conversely, if $\alpha^*$ is small, the effective equation enters into a Stokes regime. We will confirm these homogenization results by building and estimating correctors.

**2.2. Construction of correctors.** To homogenize the fine-scale system (1) to the averaged system (3), we employ estimating correctors as used in [3, 10, 11]. This method, compared to general convergence methods (cf. [1] and references therein), will allow us to carefully examine the relationship between the scale of the oscillation $\varepsilon$ and the $\delta$-parameter related to contrast $\kappa$. We begin by utilizing the two-scale asymptotic expansions as in [13, 14]. Again, letting $y = x/\varepsilon$, then derivatives transform as $\nabla \to \nabla_x + \frac{1}{\varepsilon}\nabla_y$. We expand pressure and velocity as

$$\begin{aligned} p_\varepsilon(x,y) &= p_0(x) + \varepsilon p_1(x,y) + \cdots, \\ u_\varepsilon(x,y) &= \varepsilon^2(u_0(x,y) + \varepsilon u_1(x,y) + \cdots). \end{aligned}$$

More precisely, we may write the pressures as

$$p_0(x) = \bar{p}(x) \quad \text{and} \quad p_1(x,y) = Q(y)\alpha^*\bar{u}(x),$$

and zeroth-order velocity is of the form

$$u_0(x,y) = N(y)\alpha^*\bar{u}(x).$$

Here, $(Q(y), N(y))$ satisfies the rescaled Brinkman cell equation

$$\nabla_y Q(y) - \Delta_{yy} N(y) + \varepsilon^2 \alpha(y) N(y) = e \text{ in } Y, \tag{4a}$$

$$\operatorname{div}_y(N(y)) = 0 \text{ in } Y, \tag{4b}$$

where $(Q, N)$ are $y$-periodic, $e_i$ is the $i$th Euclidean unit vector, and the average of $Q$ vanishes: $\langle Q \rangle = 0$. Here, we denote the cell average $\langle \cdot \rangle = \frac{1}{|Y|}\int_Y \cdot\, dy$. The cell equation is related to the effective Brinkman coefficient by the average condition

$$\langle \varepsilon^2 \alpha N \rangle = e, \quad \langle N \rangle = (\alpha^*)^{-1}\varepsilon^{-2}. \tag{5}$$

To obtain useful estimates, we will need the first-order corrector to the velocity $u_1$. Similar to the first-order corrector used in [3], we suppose

$$u_1(x,y) = \gamma(y)\nabla_x\left(\alpha^*\bar{u}(x)\right), \tag{6}$$

where $\gamma(y)$ satisfies additional cell problems. Indeed, $\gamma$ will satisfy

$$\operatorname{div}_y(\gamma(y)) = -N(y) + \varepsilon^{-2}|Y|^{-1}(\alpha^*)^{-1} \text{ in } Y, \tag{7}$$

where $\gamma$ is $y$-periodic and $\langle\gamma\rangle = 0$. Note that $u_1$ subsequently has zero mean: $\langle u_1\rangle = 0$. The above equations have the second term on the right-hand side to satisfy a compatibility condition standard for first-order equations of this form.

The first-order corrector is chosen to be of this form because it satisfies the divergence equation. If we apply two-scale expansions to the divergence equation (1b) and collect terms of the same order with respect to $\varepsilon$, we arrive at

$$\operatorname{div}_x(u_0) + \operatorname{div}_y(u_1) = 0.$$

Indeed, by using the form of $u_1$ as in (6) and related cell equations (7), we observe that

$$\begin{aligned}\operatorname{div}_y(u_1) &= \operatorname{div}_y\left(\gamma\nabla_x\left(\alpha^*\bar{u}\right)\right) = \operatorname{div}_y\left(\gamma\right)\nabla_x\left(\alpha^*\bar{u}\right)\\ &= \left(-N(y) + \varepsilon^{-2}|Y|^{-1}(\alpha^*)^{-1}\right)\nabla_x\left(\alpha^*\bar{u}\right)\\ &= -\operatorname{div}_x(N\alpha^*\bar{u}) + \varepsilon^{-2}|Y|^{-1}\operatorname{div}_x\bar{u} = -\operatorname{div}_x u_0.\end{aligned}$$

We are now in a position to state and discuss our main estimate. We begin with a bit of notation; then we are able to state our main convergence result. First, we set some basic notation for convenience and clarity. We will need to define the following spaces and norms. We define $H(\Omega,\operatorname{div}) = \{v \in (L^2(\Omega))^d, \operatorname{div}(v) \in L^2(\Omega)\}$ and the associated norm $\|v\|_{H(\Omega,\operatorname{div})} = \|v\|_{(L^2(\Omega))^d} + \|\operatorname{div}(v)\|_{L^2(\Omega)}$. Here, $d$ is the space dimension, and, in our paper, $d = 2, 3$. The $H^1$-seminorm on $H_0^1(\Omega)$ space (zero Dirichlet data) is defined as $|v|_{H^1(\Omega)} = \|\nabla v\|_{L^2(\Omega)}$, which is equivalent to a full $H^1$-norm by applying the Poincaré inequality. For the cell solutions, we will need the periodic spaces $H^1_{\#}(Y) = \{v \in H^1(Y),\ v \text{ is } y\text{-periodic}\}$, and in general $\#$ represents periodicity. We now state our main result.

THEOREM 2.1. *Suppose $\Omega$ is a $\mathcal{C}^\infty$ bounded domain in $\mathbb{R}^d$ where $d = 2, 3$. Let $(u_\varepsilon, p_\varepsilon)$ be given by* (1) *and $(N, Q)$, and let $\gamma$ given by* (4) *and* (7)*, respectively. Let $\alpha^*$ be given by* (5)*, and, subsequently, let $(\bar{u}, \bar{p})$ be given by* (3)*. Suppose the higher regularity $f \in H^2(\Omega)$ for the given data. Finally, suppose $\alpha$ and $\alpha^*$ satisfy the contrast bounds* (2)*. Then, we have the following estimate:*

$$\left\|u_\varepsilon - \varepsilon^2(u_0 + \varepsilon u_1)\right\|_{H(\Omega,\operatorname{div})} \le C(\varepsilon\delta^{-\eta_1+3\eta_2} + \varepsilon^2\delta^{-\eta_1+4\eta_2}), \tag{8a}$$

$$\|p_\varepsilon - \bar{p}\|_{L^2(\Omega)} \le C(\varepsilon\delta^{-\eta_1+4\eta_2} + \varepsilon^2\delta^{-\eta_1+5\eta_2}), \tag{8b}$$

*where the first-order corrector is given by $u_0 + \varepsilon u_1 = N(y)\alpha^*\bar{u}(x) + \varepsilon\gamma(y)\nabla_x\left(\alpha^*\bar{u}(x)\right)$.*

*Remark.* One has to exercise caution when using the above estimate, as this estimate does not take into account the magnitude of the velocity field $u_\varepsilon$. If the magnitude of the velocity $u_\varepsilon$ is small, then (8) can, in general, be an overestimate and will not give an advantageous bound. However, the closeness of the correctors can be approximated and the fine-scale solution can be derived from estimate (8) for a certain range of $\delta$ and $\varepsilon$.

To elucidate the meaning of the corrector estimate result, it is helpful to give some values to the contrast. In addition, we would like to understand the relationship between the scales and contrast parameters. Assume we have the case where $\eta_1 = 0$ and $\eta_2 = -1$. We suppose the relationship between the scales and contrast are such that $\delta = \varepsilon^s$ for some $s \geq 0$. Here, the contrast value is given by $\kappa = \varepsilon^{-s}$. From the estimate (8a), we obtain the estimate

$$\left\|u_\varepsilon - \varepsilon^2(u_0 + \varepsilon u_1)\right\|_{H(\Omega,\mathrm{div})} \leq C\left(\varepsilon^{(-3s+1)} + \varepsilon^{(-4s+2)}\right).$$

If the Darcy slow flow regime is significantly larger than the Stokesian regime, then it can be argued that $u_\varepsilon \approx O(\varepsilon^s)$, and similarly for the corrector $\varepsilon^2(u_0 + \varepsilon u_1)$. In this case, normalizing the velocity to this scale, the estimate becomes

$$\frac{1}{\varepsilon^s}\left\|u_\varepsilon - \varepsilon^2(u_0 + \varepsilon u_1)\right\|_{H(\Omega,\mathrm{div})} \leq C\left(\varepsilon^{(-4s+1)} + \varepsilon^{(-5s+2)}\right).$$

We find the value of $s$ so that the velocity corrector converges in $\varepsilon$. Thus, if $s \in [0, \frac{1}{4})$ and $\delta = \varepsilon^s$, the above estimate will converge in $\varepsilon$. We see here that the contrast in the media must grow slower than the scales for these estimates to remain valid.

**3. Numerical implementation.** In this section, we present numerical results for the correctors constructed in the previous sections. We will validate the convergence result in Theorem 2.1 for two different coefficients $\alpha$. Recall that, to obtain theoretical estimates, we need higher-order terms of the corrector. To obtain the estimates for our numerical results, only our first order of the corrector $\varepsilon^2 u_0$ is needed. We present our results in a few figures and compare convergence results in the tables.

For our numerical implementation, we consider the Brinkman equation in the unit square $\Omega = [0,1]^2$ and, subsequently, $\Omega = Y$. To generate a complex flow, we use the following source term for all the high-contrast coefficients given by

$$f(x_1, x_2) = (f_1(x_1, x_2), f_2(x_1, x_2)),$$

where

$$\begin{aligned} f_1(x_1, x_2) &= (\cos x_1 \cos x_2 + 2\pi(2(1-x_1)^2 - 8x_1(1-x_1) + 2x_1^2)\sin(\pi x_2)\cos(\pi x_2) \\ &\quad - x_1^2(1-x_1)^2\pi(2\pi)^2\sin(2\pi x_2)), \\ f_2(x_1, x_2) &= (-\sin x_1 \sin x_2 - (2x_1(1-x_1)^2 + 2x_1^2(x_1-1))2\pi^2(\cos^2(\pi x_2) - \sin^2(\pi x_2)) \\ &\quad - (24x_1 - 12)\sin^2(\pi x_2)) \end{aligned}$$

for $(x_1, x_2) \in [0,1]^2$.

We will use two different coefficients: the first is Stokes flow in the fractures with square Darcy inclusions, and the second is the converse: Darcy flow with Stokes flow vuggs. To this end, we define the coefficients on the unit cell as

$$\alpha_1(y) = \begin{pmatrix} \delta^{\eta_1} & 0 \\ 0 & \delta^{\eta_1} \end{pmatrix}, \quad \alpha_2(y) = \begin{pmatrix} \delta^{\eta_2} & 0 \\ 0 & \delta^{\eta_2} \end{pmatrix}$$

for $\eta_1 = 0$ and $\eta_2 = -1$. To give the microstructure two distinct regions, we define the rectangle $U = [\frac{1}{3}, \frac{2}{3}]^2$. We now construct the coefficients and summarize this construction in Figure 1 for $\varepsilon = \frac{1}{8}$. We present them here on the unit cell and then scale and translate them in the figures. For the first coefficient rescaled in Figure

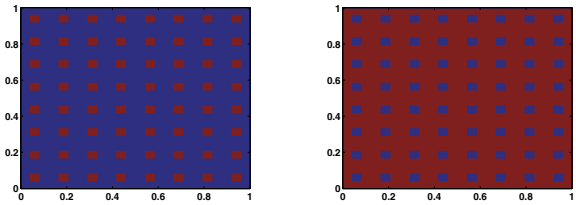

(a) (b)

FIG. 1. *Two fine-scale high-contrast coefficients $\alpha$ for $\varepsilon = \frac{1}{8}$. Here we have* (a) *Stokes flow in fractures with Darcy inclusions and* (b) *Darcy flow with Stokesian vuggs.*

1(a), we let $\alpha(y) = \alpha_1(y)$ for $y \in Y\backslash U$ and $\alpha(y) = \alpha_2(y)$ for $y \in U$. Inverting this procedure, we let $\alpha(y) = \alpha_2(y)$ for $y \in Y\backslash U$ and $\alpha(y) = \alpha_1(y)$ for $y \in U$. This is presented in Figure 1(b).

For convergence results, we will investigate the behavior of the first-order corrector error, $u_\varepsilon - \varepsilon^2 u_0$, as we decrease the contrast parameter $\delta$ and scales $\varepsilon$. As stated earlier, the second-order term, $u_1$, is not needed for the computational estimates and is only utilized in the theoretical corrector estimates. The errors are given in an $L^2$-norm, $\alpha$-norm, and $H^1$-norm, where the $\alpha$-norm is defined as

$$\|u\|_\alpha = \left( \int_\Omega u^T \alpha u \right)^{\frac{1}{2}}.$$

We will present absolute and relative errors in these norms. We show that, using the correctors discussed above, we achieve an error estimate and rates depending on the pore size $\varepsilon$ and the high-contrast $\delta$ as in Theorem 2.1.

For our simulation, we divide our domain into $180 \times 180$ equal square elements and then divide each square into two triangles. We will use a stable Taylor–Hood element of the kind $\mathbb{P}^2/\mathbb{P}^0$, quadratic for velocity and constant for pressure. Recall that $\eta_1 = 0$, $\eta_2 = -1$ in all the numerical tests. To visualize the solutions, we compute in the first geometry in Figure 1(a) for $\delta = 0.1$. In Figure 2, we display each component of the fine-scale solution and first-order corrector. Visually, the agreement between the fine scale and corrector is acceptable, as can be verified by the relative errors. However, as we decrease $\delta$, we will observe a degradation in the quality of the corrector in agreement with the main theorem estimate.

We consider the coefficients as shown in Figure 1. First, we vary $\delta$ between 0.5 to 0.02, fixing $\varepsilon$. The results are presented in Tables 1 and 2. The first column of the tables shows the value of $\delta$. Again, these values provide various high-contrast coefficients. The next three columns display the absolute error between the fine-scale solution and first-order corrector constructed above. We present absolute error in the form of an $L^2$-norm, an $L^2$ $\alpha$-weighted-norm, and an $H^1$-norm. Similarly, the last three columns show the relative error in those norms. The final column shows the calculated $\eta^*$ from the relation $\alpha^* \approx \delta^{\eta^*}$. Using the result of Theorem 2.1, but with $\alpha^* \approx \delta^{\eta^*}$, we have

$$\left\| u_\varepsilon - \varepsilon^2 u_0 \right\|_{H^1(\Omega)} \leq C(\varepsilon \delta^{\eta_2 + 2\eta_*} + \varepsilon^2 \delta^{2\eta_2 + 2\eta_*}). \tag{9}$$

From this inequality and the tables we can compare theoretical $\delta$-rates. For the first medium in Figure 1(a), we observe numerical rates of the order $-1$ compared to

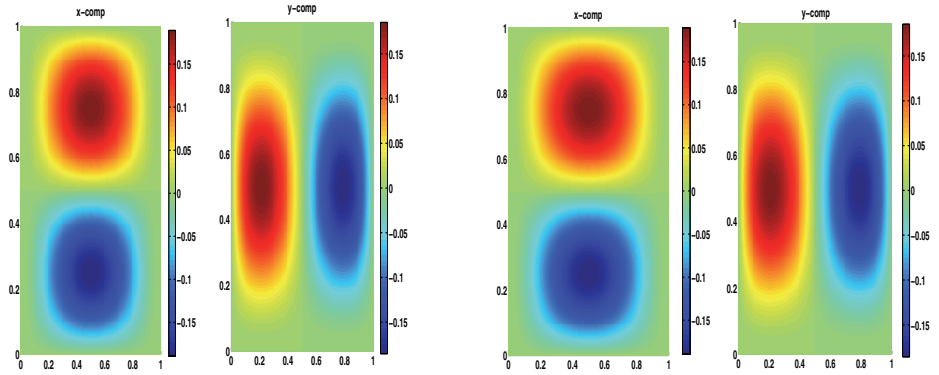


(a) $u_\varepsilon$ (b) $\varepsilon^2 u_0$

FIG. 2. *The components of the fine-scale solution, $u_\varepsilon$, and first-order corrector, $\varepsilon^2 u_0$, for the coefficient in Figure* 1(a) *with contrast $\delta = 0.1$.*

TABLE 1

*Convergence results for the medium depicted in Figure* 1(a). *Fixing $\varepsilon$ and varying $\delta$. The absolute and relative errors are presented.*

| $\delta$ | $\|u_\varepsilon - \varepsilon^2 u_0\|_{L^2(\Omega)}$ | $\|u_\varepsilon - \varepsilon^2 u_0\|_\alpha$ | $\|u_\varepsilon - \varepsilon^2 u_0\|_{H^1(\Omega)}$ | $\frac{\|u_\varepsilon - \varepsilon^2 u_0\|_{L^2(\Omega)}}{\|u_\varepsilon\|_{L^2(\Omega)}}$ | $\frac{\|u_\varepsilon - \varepsilon^2 u_0\|_\alpha}{\|u_\varepsilon\|_\alpha}$ | $\frac{\|u_\varepsilon - \varepsilon^2 u_0\|_{H^1(\Omega)}}{\|u_\varepsilon\|_{H^1(\Omega)}}$ | $\eta_*$ |
|---|---|---|---|---|---|---|---|
| 0.5 | $1.1807e-5$ | $1.1944e-5$ | $3.0401e-4$ | $9.8506e-3\%$ | $9.4832e-3\%$ | $3.4431e-2\%$ | $-0.1469$ |
| 0.1 | $1.0303e-4$ | $1.1323e-4$ | $2.6893e-3$ | $0.0873\%$ | $0.0689\%$ | $0.3093\%$ | $-0.2933$ |
| 0.02 | $4.8468e-4$ | $6.9720e-4$ | $1.3482e-2$ | $0.4419\%$ | $0.2578\%$ | $1.6668\%$ | $-0.4684$ |

TABLE 2

*Convergence results for the medium depicted in Figure* 1(b). *Fixing $\varepsilon$ and varying $\delta$. The absolute and relative errors are presented.*

| $\delta$ | $\|u_\varepsilon - \varepsilon^2 u_0\|_{L^2(\Omega)}$ | $\|u_\varepsilon - \varepsilon^2 u_0\|_\alpha$ | $\|u_\varepsilon - \varepsilon^2 u_0\|_{H^1(\Omega)}$ | $\frac{\|u_\varepsilon - \varepsilon^2 u_0\|_{L^2(\Omega)}}{\|u_\varepsilon\|_{L^2(\Omega)}}$ | $\frac{\|u_\varepsilon - \varepsilon^2 u_0\|_\alpha}{\|u_\varepsilon\|_\alpha}$ | $\frac{\|u_\varepsilon - \varepsilon^2 u_0\|_{H^1(\Omega)}}{\|u_\varepsilon\|_{H^1(\Omega)}}$ | $\eta_*$ |
|---|---|---|---|---|---|---|---|
| 0.5 | $1.1481e-5$ | $1.6142e-5$ | $2.9122e-4$ | $9.7197e-3\%$ | $9.9256e-3\%$ | $3.4383e-2\%$ | $-0.9205$ |
| 0.1 | $8.1690e-5$ | $2.5580e-4$ | $2.3551e-3$ | $0.0782\%$ | $0.0814\%$ | $0.3057\%$ | $-0.9559$ |
| 0.02 | $1.9821e-4$ | $1.3716e-3$ | $7.8319e-3$ | $0.2997\%$ | $0.3096\%$ | $1.5909\%$ | $-0.9716$ |

the theoretical rates of $-3$ computed from result (9) in section 2.2. For the second medium, we observe numerical rates again of the order $-1$ compared to the theoretical rates of $-4$.

The second set of tests is comprised of the $\varepsilon$ convergence of the corrector estimate. We fix $\delta = 0.1$ and let $\varepsilon$ vary. These results are displayed in Tables 3 and 4. Similarly, the first columns are for the $\varepsilon$ values of 0.25 to 0.1. We then display the absolute and relative errors. In both examples we observe rates that are close to this theoretical rate. Compare this to the $\delta$-rates, which seem to perform much better than the theory in these two examples.

To demonstrate the pressure estimates we implement a few numerical tests to support the theoretical estimate (8b). We display the numerical results for pressure only corresponding to the first permeability field in Figure 1(a). The fine-scale pressure solution $p_\varepsilon$ and zeroth-order corrector $\bar{p}$ are shown in Figure 3. One observes that $\bar{p}$ does not contain oscillations and appears to be a good approximation of $p_\varepsilon$.

In the following, we perform several numerical tests for fixed $\varepsilon$ and $\delta$, respectively, and the results are displayed in Tables 5 and 6. Calculating the convergence rate with respect to $\delta$ based on the data in Table 5, we obtain a rate of $-1.2$, compared to the

TABLE 3

*Convergence results for the medium depicted in Figure* 1(a). *Fixing* $\delta$ *and varying* $\varepsilon$. *The absolute and relative errors are presented.*

| $\varepsilon$ | $\|u_\varepsilon - \varepsilon^2 u_0\|_{L^2(\Omega)}$ | $\|u_\varepsilon - \varepsilon^2 u_0\|_\alpha$ | $\|u_\varepsilon - \varepsilon^2 u_0\|_{H^1(\Omega)}$ | $\frac{\|u_\varepsilon - \varepsilon^2 u_0\|_{L^2(\Omega)}}{\|u_\varepsilon\|_{L^2(\Omega)}}$ | $\frac{\|u_\varepsilon - \varepsilon^2 u_0\|_\alpha}{\|u_\varepsilon\|_\alpha}$ | $\frac{\|u_\varepsilon - \varepsilon^2 u_0\|_{H^1(\Omega)}}{\|u_\varepsilon\|_{H^1(\Omega)}}$ |
|---|---|---|---|---|---|---|
| 0.25 | $3.4550e-4$ | $6.6324e-4$ | $6.9607e-3$ | 0.2930% | 0.3979% | 0.8014% |
| 0.16 | $1.9298e-4$ | $3.7727e-4$ | $4.8252e-3$ | 0.1638% | 0.2250% | 0.5577% |
| 0.1 | $1.0303e-4$ | $1.1323e-4$ | $2.6893e-3$ | 0.0873% | 0.0689% | 0.3093% |

TABLE 4

*Convergence results for the medium depicted in Figure* 1(b). *Fixing* $\delta$ *and varying* $\varepsilon$. *The absolute and relative errors are presented.*

| $\varepsilon$ | $\|u_\varepsilon - \varepsilon^2 u_0\|_{L^2(\Omega)}$ | $\|u_\varepsilon - \varepsilon^2 u_0\|_\alpha$ | $\|u_\varepsilon - \varepsilon^2 u_0\|_{H^1(\Omega)}$ | $\frac{\|u_\varepsilon - \varepsilon^2 u_0\|_{L^2(\Omega)}}{\|u_\varepsilon\|_{L^2(\Omega)}}$ | $\frac{\|u_\varepsilon - \varepsilon^2 u_0\|_\alpha}{\|u_\varepsilon\|_\alpha}$ | $\frac{\|u_\varepsilon - \varepsilon^2 u_0\|_{H^1(\Omega)}}{\|u_\varepsilon\|_{H^1(\Omega)}}$ |
|---|---|---|---|---|---|---|
| 0.25 | $3.0362e-4$ | $8.2020e-4$ | $6.1312e-3$ | 0.2905% | 0.2618% | 0.7948% |
| 0.16 | $1.6593e-4$ | $4.4380e-4$ | $4.2612e-3$ | 0.1587% | 0.1417% | 0.5523% |
| 0.1 | $8.1690e-5$ | $2.5580e-4$ | $2.3551e-3$ | 0.0782% | 0.0814% | 0.3057% |

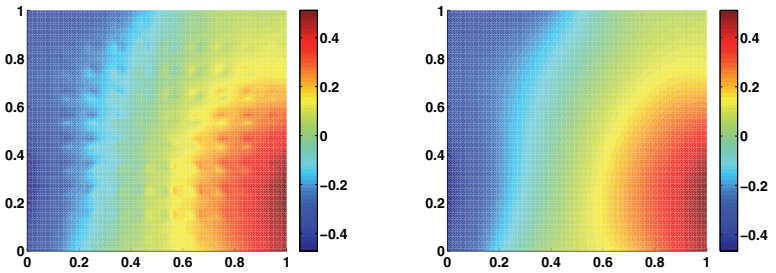


(a) $p_\varepsilon$ (b) $\bar{p}$

FIG. 3. *The fine-scale solution,* $p_\varepsilon$, *and zeroth-order corrector,* $\bar{p}$, *for the coefficient in Figure* 1(a) *with contrast* $\delta = 0.1$.

theoretical rate of $-4$ from (9). Similarly, we can derive the convergence rate of the pressure with respect to $\varepsilon$ from Table 6, and it is around the theoretical convergence rate of order 1, assuming we are not in the small velocity regime.

**4. Analysis.** In this section, we will prove the estimates in Theorem 2.1. This is accomplished by first constructing the boundary correction of the first-order corrector. Then, the residual equation is derived. From here, we will need to estimate the divergence and residual of the boundary correction. Using the auxiliary estimates from the appendix, we make careful estimates of residual quantities and arrive at our final estimates.

It is important to note in the following analysis that the Poincaré inequality used in this discussion differs from the case of perforated domains. In the case of perforated domains with zero Dirichlet data, an extra $\varepsilon$ is gained from the Poincaré inequality [10]. Indeed, letting $\Omega_\varepsilon$ be a perforated domain and letting $\phi \in H_0^1(\Omega_\varepsilon)$, we have

$$\|\phi\|_{L^2(\Omega_\varepsilon)} \leq \varepsilon C \|\nabla \phi\|_{L^2(\Omega_\varepsilon)}. \tag{10}$$

Thus, this allows sharper estimates to be obtained in the small velocity regime of Stokes homogenization past obstacles. In our unperforated setting, to obtain sharp estimates one needs to find appropriate Poincaré-type estimates that can deal with

TABLE 5

*Convergence results for the medium depicted in Figure* 1(a). *Fixing* $\varepsilon = 0.1$ *and varying* $\delta$. *The absolute and relative errors of the pressure are presented.*

| $\delta$ | $\|p_\varepsilon - \bar{p}\|_{L^2(\Omega)}$ | $\|p_\varepsilon\|_{L^2(\Omega)}$ | $\frac{\|p_\varepsilon - \bar{p}\|_{L^2(\Omega)}}{\|p_\varepsilon\|_{L^2(\Omega)}}$ |
|---|---|---|---|
| 0.5 | 0.0003 | 0.2208 | 0.1359% |
| 0.1 | 0.0027 | 0.2210 | 1.2015% |
| 0.05 | 0.0133 | 0.2230 | 5.9837% |

TABLE 6

*Convergence results for the medium depicted in Figure* 1(a). *Fixing* $\delta = 0.1$ *and varying* $\varepsilon$. *The absolute and relative errors of the pressure are presented.*

| $\epsilon$ | $\|p_\varepsilon - \bar{p}\|_{L^2(\Omega)}$ | $\|p_\varepsilon\|_{L^2(\Omega)}$ | $\frac{\|p_\varepsilon - \bar{p}\|_{L^2(\Omega)}}{\|p_\varepsilon\|_{L^2(\Omega)}}$ |
|---|---|---|---|
| 0.25 | 0.0073 | 0.2210 | 3.3148% |
| 0.16 | 0.0046 | 0.2210 | 2.0989% |
| 0.1 | 0.0027 | 0.2210 | 1.2015% |

low velocities in some regions. Perhaps in this setting, with more assumptions on the geometry, sharper bounds can be obtained in this regime.

**4.1. Boundary correction.** Note that fine-scale velocity $u_\varepsilon$ and homogenized velocity $\bar{u}$ satisfy zero Dirichlet boundary conditions. However, the corrector $u_0 + \varepsilon u_1$ is not necessarily zero on the boundary. To account for this, we must adapt the corrector near the boundary. We utilize a presentation similar to that in [3, 10].

To achieve this goal, we will need the cut-off function $\zeta^\varepsilon$ corresponding to $\partial\Omega$. Here, $\zeta^\varepsilon = 1$ on $\partial\Omega$ and $\text{supp}(\zeta^\varepsilon) \subset \{x \in \bar{\Omega}; \text{dist}(x, \partial\Omega) \leq \varepsilon\}$. With regularity conditions $\zeta^\varepsilon \in C^2(\bar{\Omega})$ for $0 \leq l \leq 2$ we have

$$||D^l \zeta^\epsilon||_{L^\infty(\Omega)} \leq C\varepsilon^{-l}. \tag{11}$$

In addition, using (11) and the fact that $|\text{supp}(\zeta^\varepsilon)| = O(\varepsilon)$, and also by application of Hölder's inequality, we have the estimate for derivatives of the cut-off function in $L^q(\Omega)$ given by

$$\left\|D^l \zeta^\varepsilon\right\|_{L^q(\Omega)} \leq C|\text{supp}(\zeta^\varepsilon)|^{1/q} \left\|D^l \zeta^\varepsilon\right\|_{L^\infty(\Omega)} \leq C\varepsilon^{1/q-l}. \tag{12}$$

With this cut-off function we can now write the boundary corrector for velocity as

$$\mathcal{U}^\varepsilon = \varepsilon^2 N \alpha^* \bar{u} + \varepsilon^3 (1 - \zeta^\varepsilon) \gamma \nabla_x (\alpha^* \bar{u}) \tag{13}$$

and for pressure as

$$\mathcal{P}^\varepsilon = \bar{p} + \varepsilon Q \alpha^* \bar{u}. \tag{14}$$

Note that for $x \in \partial\Omega$, $\mathcal{U}^\varepsilon = 0$ since $\bar{u} = 0$ and $\zeta^\varepsilon = 1$ on $\partial\Omega$. Also, note that on average $\langle \mathcal{U}^\varepsilon \rangle = \bar{u}$ and $\langle \mathcal{P}^\varepsilon \rangle = \bar{p}$.

Using the above boundary correctors, we will obtain our estimates in the standard way by estimating residuals. Indeed, let $z_\varepsilon = u_\varepsilon - \mathcal{U}^\varepsilon$ and $\Xi_\varepsilon = p_\varepsilon - \mathcal{P}^\varepsilon$. Applying the differences to the fine-scale Brinkman equation (1) we obtain

$$\nabla \Xi_\varepsilon - \Delta z_\varepsilon + \alpha \left(\frac{x}{\varepsilon}\right) z_\varepsilon = \Psi^\varepsilon \text{ in } \Omega,$$
$$\text{div}\,(z_\varepsilon) = -\text{div}\,(\mathcal{U}^\varepsilon) \text{ in } \Omega, \quad z_\varepsilon = 0 \text{ on } \partial\Omega,$$

where the residual is given by

$$\Psi^\varepsilon = f - \nabla \mathcal{P}^\varepsilon + \Delta \mathcal{U}^\varepsilon - \alpha\,(x/\varepsilon)\,\mathcal{U}^\varepsilon. \tag{15}$$

We will now carefully estimate $\|\mathrm{div}\,(\mathcal{U}^\varepsilon)\|_{L^2(\Omega)}$ and $\|\Psi^\varepsilon\|_{H^{-1}(\Omega)}$, therefore, we can use estimate (24) and Corollary 6.3 to get Theorem 2.1.

**4.2. Estimation of div($\mathcal{U}^\epsilon$).** We begin with estimate of the divergence of the boundary corrector. Taking the two-scale divergence as $\mathrm{div}(\cdot) \to \mathrm{div}_x(\cdot) + \frac{1}{\varepsilon}\mathrm{div}_y(\cdot)$, we have

$$\begin{aligned}\frac{1}{\varepsilon^2}\mathrm{div}(\mathcal{U}^\varepsilon) =& \mathrm{div}(N\alpha^{*-1}\bar{u}) + \varepsilon(1-\zeta^\varepsilon)\gamma\nabla(\nabla_x(\alpha^{*-1}\bar{u})) + \varepsilon\mathrm{div}_x((1-\zeta^\varepsilon)\gamma)\nabla_x(\alpha^{*-1}\bar{u})\\ &= (N-\varepsilon^{-2}\alpha^{*-1})\nabla_x(\alpha^{*-1}\bar{u})\zeta^\varepsilon + \varepsilon(1-\zeta^\varepsilon)\gamma\nabla(\nabla_x(\alpha^{*-1}\bar{u}))\\ &- \varepsilon\mathrm{div}_x\zeta^\varepsilon\gamma\nabla_x(\alpha^{*-1}\bar{u}) + \varepsilon^{-2}(1-\zeta^\varepsilon)\alpha^{*-1}\nabla_x(\alpha^{*-1}\bar{u}).\end{aligned}$$

In view of the relation $\varepsilon^{-2}\alpha^{*-1} = \langle N\rangle$ and $\mathrm{div}(\bar{u}) = 0$, we can deduce that

$$\begin{aligned}\varepsilon^{-2}\alpha^{*-1}\nabla_x(\alpha^{*-1}\bar{u}) &= \langle N\rangle\nabla_x(\alpha^{*-1}\bar{u})\\ &= \mathrm{div}(\langle N\rangle\alpha^{*-1}\bar{u}) = \mathrm{div}(\varepsilon^{-2}\bar{u}) = \varepsilon^{-2}\mathrm{div}(\bar{u}) = 0.\end{aligned}$$

Thus,

$$\begin{aligned}\frac{1}{\varepsilon^2}\mathrm{div}(\mathcal{U}^\varepsilon) &= (N-\varepsilon^{-2}\alpha^{*-1})\nabla_x(\alpha^{*-1}\bar{u})\zeta^\varepsilon + \varepsilon(1-\zeta^\varepsilon)\gamma\nabla(\nabla_x(\alpha^{*-1}\bar{u}))\\ &- \varepsilon\mathrm{div}_x\zeta^\varepsilon\gamma\nabla_x(\alpha^{*-1}\bar{u}).\end{aligned}$$

We now estimate each term. Recall, throughout these estimates, that $\delta^{\eta_2}$ is the upper bound of $\alpha^*$. Applying Hölder's inequality, a Sobolev embedding, and the Poincaré inequality, we arrive at

$$\begin{aligned}\left\|(N-\varepsilon^{-2}\alpha^{*-1})\nabla_x(\alpha^{*-1}\bar{u})\zeta^\varepsilon\right\|_{L^2(\Omega)} &= \|(N-\langle N\rangle)\nabla_x(\alpha^{*-1}\bar{u})\zeta^\varepsilon\|_{L^2(\Omega)}\\ &\le C\,\|\nabla N\|_{L^2(Y)}\,\delta^{\eta_2}\,\|\nabla\bar{u}\|_{L^\infty(\Omega)}\,\|\zeta^\varepsilon\|_{L^\infty(\Omega)}\\ &\le C\,\|\nabla N\|_{L^2(Y)}\,\delta^{\eta_2}\,\|\nabla\bar{u}\|_{H^2(\Omega)}\,\|\zeta^\varepsilon\|_{L^\infty(\Omega)}\\ &\le C\delta^{-\eta_1+3\eta_2}.\end{aligned}$$

Above, we applied the estimates of $\|\nabla\bar{u}\|_{H^2(\Omega)}$ and $\|\nabla_y N\|_{L^2(Y)}$ from the inequalities (21) and (27), respectively. By application of Hölder's inequality and Sobolev embeddings we obtain

$$\begin{aligned}\|\varepsilon(1-\zeta^\varepsilon)\gamma\nabla(\nabla_x(\alpha^{*-1}\bar{u}))\|_{L^2(\Omega)} &\le C\varepsilon\delta^{\eta_2}\,\|\zeta^\varepsilon-1\|_{L^\infty(\Omega)}\,\|\gamma\|_{L^4(Y)}\,\left\|\nabla^2\bar{u}\right\|_{L^4(\Omega)}\\ &\le C\varepsilon\delta^{\eta_2}\,\|\zeta^\varepsilon-1\|_{L^\infty(\Omega)}\,\|\gamma\|_{H^1(Y)}\,\|\bar{u}\|_{H^3(\Omega)}\\ &\le C\varepsilon\delta^{-\eta_1+3\eta_2}.\end{aligned}$$

Here, we used estimates of $\|\bar{u}\|_{H^3(\Omega)}$ from inequality (21) and $\|\gamma\|_{H^1(\Omega)}$ from inequality (34) in the appendix. For the last term, again applying the same techniques, we can obtain

$$\begin{aligned}\|-\varepsilon\mathrm{div}_x\zeta^\varepsilon\gamma\nabla_x(\alpha^{*-1}\bar{u})\|_{L^2(\Omega)} &\le C\varepsilon\delta^{\eta_2}\,\|\mathrm{div}_x\zeta^\varepsilon\|_{L^\infty(\Omega)}\,\|\gamma\|_{L^4(Y)}\,\|\nabla\bar{u}\|_{L^4(\Omega)},\\ &\le C\varepsilon\delta^{\eta_2}\,\|\mathrm{div}_x\zeta^\varepsilon\|_{L^\infty(\Omega)}\,\|\gamma\|_{H^1(Y)}\,\|\bar{u}\|_{H^3(\Omega)}\\ &\le C\delta^{-\eta_1+3\eta_2}.\end{aligned}$$

Above, we used estimates of $\|\bar{u}\|_{H^3(\Omega)}$ and $\|\gamma\|_{H^1(Y)}$ from inequalities (21) and (34), respectively. Collecting those three terms above and using the assumption that $\eta_2 < 0$,

$$\|\mathrm{div}(\mathcal{U}^\varepsilon)\|_{L^2(\Omega)} \leq C\varepsilon^2\delta^{-\eta_1+3\eta_2}. \tag{16}$$

**4.3. Estimation of residual $\boldsymbol{\Psi^\varepsilon}$.** We shall expand the residual (15) and then estimate the inner product to obtain a bound on the $H^{-1}$-norm. Note that here we do not use two-scale derivatives, so the scaling must be carefully scrutinized:

$$\begin{aligned}\Psi^\varepsilon &= f - \nabla\bar{p} - \varepsilon\nabla Q\alpha^*\bar{u} - \varepsilon Q\nabla\left(\alpha^*\bar{u}\right)\\ &\quad + \Delta\left(\varepsilon^2 N\alpha^*\bar{u}\right) + \Delta\left(\varepsilon^3\gamma\nabla(\alpha^*\bar{u})(1-\zeta^\varepsilon)\right)\\ &\quad - \alpha(x/\varepsilon)\left(\varepsilon^2 N\alpha^*\bar{u} + \varepsilon^3\gamma\nabla(\alpha^*\bar{u})(1-\zeta^\varepsilon)\right).\end{aligned}$$

Putting the $\gamma$ terms toward the end and collecting the cell terms, we have

$$\begin{aligned}\Psi^\varepsilon &= f - \nabla\bar{p} - \left(\varepsilon\nabla Q - \varepsilon^2\Delta N + \varepsilon^2\alpha(x/\varepsilon)N\right)\alpha^*\bar{u}\\ &\quad - \varepsilon Q\nabla(\alpha^*\bar{u}) + 2\varepsilon^2\nabla N\nabla(\alpha^*\bar{u}) + \varepsilon^2 N\Delta(\alpha^*\bar{u})\\ &\quad + \Delta\left(\varepsilon^3\gamma\nabla(\alpha^*\bar{u})(1-\zeta^\varepsilon)\right) - \alpha(x/\varepsilon)\left(\varepsilon^3\gamma\nabla(\alpha^*\bar{u})(1-\zeta^\varepsilon)\right).\end{aligned}$$

Using the cell relation (4), we have $\varepsilon\nabla Q - \varepsilon^2\Delta N + \varepsilon^2\alpha(x/\varepsilon)N = e$, and using the homogenized Brinkman equation (3), we have the relation $f - \nabla\bar{p} = \alpha^*\bar{u} - \Delta\bar{u}$. From these relations we have

$$\begin{aligned}\Psi^\varepsilon &= (\varepsilon^2 N\alpha^* - 1)\Delta\bar{u} + (2\varepsilon^2\nabla N\nabla(\alpha^*\bar{u}) - \varepsilon Q\nabla(\alpha^*\bar{u}))\\ &\quad + \Delta\left(\varepsilon^3\gamma\nabla(\alpha^*\bar{u})(1-\zeta^\varepsilon)\right) - \alpha(x/\varepsilon)\left(\varepsilon^3\gamma\nabla(\alpha^*\bar{u})(1-\zeta^\varepsilon)\right).\end{aligned}$$

Organizing the terms, we can write them as

$$\begin{aligned}\Psi_1^\varepsilon &= (\varepsilon^2 N\alpha^* - 1)\Delta\bar{u},\\ \Psi_2^\varepsilon &= 2\varepsilon^2\nabla N\nabla(\alpha^*\bar{u}) - \varepsilon Q\nabla(\alpha^*\bar{u}),\\ \Psi_3^\varepsilon &= \varepsilon^3\gamma\nabla(\alpha^*\bar{u})(1-\zeta^\varepsilon),\\ \Psi_4^\varepsilon &= \alpha(x/\varepsilon)\varepsilon^3\gamma\nabla(\alpha^*\bar{u})(1-\zeta^\varepsilon).\end{aligned}$$

Multiplying by $\phi \in H_0^1(\Omega)^d$ and integrating the third term by parts, we gain

$$\int_\Omega \Psi^\varepsilon\phi = \int_\Omega \Psi_1^\varepsilon\phi + \int_\Omega \Psi_2^\varepsilon\phi - \int_\Omega \nabla\Psi_3^\varepsilon\nabla\phi - \int_\Omega \Psi_4^\varepsilon\phi.$$

We estimate term by term. By cell equation (4) and the standard inequalities, we obtain

$$\begin{aligned}\left|\int_\Omega \Psi_1^\varepsilon\phi\right| &\leq \int_\Omega |(\varepsilon^2 N\alpha^* - 1)\Delta\bar{u}\phi| = \int_\Omega |\varepsilon^2(N - \langle N\rangle)\alpha^*\Delta\bar{u}\phi|\\ &\leq \varepsilon^2\delta^{\eta_2}\|\nabla N\|_{L^2(\Omega)}\|\nabla\bar{u}\|_{H^2(\Omega)}\|\phi\|_{H^1(\Omega)}\\ &\leq C\varepsilon^2\delta^{-\eta_1+3\eta_2}\|\phi\|_{H^1(\Omega)}.\end{aligned}$$

Here, estimates of $\|\nabla \bar{u}\|_{H^2(\Omega)}$ and $\|\nabla N\|_{L^2(Y)}$ given by (21) and (26) from the appendix were used. Using Hölder's inequality and Sobolev embedding yields

$$\begin{aligned}\left|\int_\Omega \Psi_2^\varepsilon \phi\right| &\le \varepsilon \int_\Omega |2\nabla_y N \nabla(\alpha^* \bar{u})\phi| + |Q\nabla(\alpha^* \bar{u})\phi| \\ &\le \varepsilon\delta^{\eta_2}(\|2\nabla_y N\|_{L^2(Y)} + \|Q\|_{L^2(Y)})\,\|\nabla \bar{u}\|_{L^4(\Omega)}\,\|\phi\|_{L^4(\Omega)} \\ &\le \varepsilon\delta^{\eta_2}(\|2\nabla_y N\|_{L^2(Y)} + \|Q\|_{L^2(Y)})\,\|\bar{u}\|_{H^2(\Omega)}\,\|\phi\|_{H^1(\Omega)}\,.\end{aligned}$$

Now, using the estimates of $\|\bar{u}\|_{H^2(\Omega)}$, $\|\nabla N\|_{L^2(Y)}$, and $\|Q\|_{L^2(Y)}$ from (21), (26), and (28), respectively, we obtain the bound

$$\left|\int_\Omega \Psi_2^\varepsilon \phi\right| \le C\varepsilon\delta^{-\eta_1+3\eta_2}\,\|\phi\|_{H^1(\Omega)}\,.$$

Again, using standard inequalities, we can get

$$\begin{aligned}\left|\int_\Omega \nabla\Psi_3^\varepsilon \nabla\phi\right| &\le \int_\Omega |\nabla\left(\varepsilon^3\gamma\nabla(\alpha^*\bar{u})(1-\zeta^\varepsilon)\right)\nabla\phi|, \\ &\le \varepsilon^2(\varepsilon\,\|\gamma\|_{L^2(Y)}\,\|1-\zeta^\varepsilon\|_{L^\infty(\Omega)}\,\left\|\nabla^2(\alpha^*\bar{u})\right\|_{L^\infty(\Omega)} \\ &+ \|\nabla\gamma\|_{L^2(Y)}\,\|1-\zeta^\varepsilon\|_{L^\infty(\Omega)}\,\|\nabla(\alpha^*\bar{u})\|_{L^\infty(\Omega)} \\ &+ \varepsilon\,\|\gamma\|_{L^2(Y)}\,\|\nabla\zeta^\varepsilon\|_{L^\infty(\Omega)}\,\|\nabla(\alpha^*\bar{u})\|_{L^\infty(\Omega)})\,\|\phi\|_{H^1(\Omega)} \\ &\le \varepsilon^2(\varepsilon\delta^{\eta_2}\,\|\gamma\|_{L^2(Y)}\,\|1-\zeta^\varepsilon\|_{L^\infty(\Omega)}\,\|\bar{u}\|_{H^4(\Omega)} \\ &+ \delta^{\eta_2}\,\|\nabla\gamma\|_{L^2(Y)}\,\|1-\zeta^\varepsilon\|_{L^\infty(\Omega)}\,\|\bar{u}\|_{H^3(\Omega)} \\ &+ \delta^{\eta_2}\,\|\gamma\|_{L^2(Y)}\,\|\bar{u}\|_{H^3(\Omega)})\,\|\phi\|_{H^1(\Omega)}\,.\end{aligned}$$

We use the estimate of $\|\gamma\|_{H^1(Y)}$ given by (34). In addition, for $\|\bar{u}\|_{H^3(\Omega)}$ and $\|\bar{u}\|_{H^4(\Omega)}$, we use (21) from the appendix and obtain

$$\left|\int_\Omega \nabla\Psi_3^\varepsilon \nabla\phi\right| \le C\varepsilon^2(\varepsilon\delta^{-\eta_1+4\eta_2} + \delta^{-\eta_1+3\eta_2})\,\|\phi\|_{H^1(\Omega)}\,.$$

Finally, we estimate the last term

$$\begin{aligned}\left|\int_\Omega \Psi_4^\varepsilon \phi\right| &\le \int_\Omega |\alpha(x/\varepsilon)\varepsilon^3\gamma\alpha^*\nabla\bar{u}(1-\zeta^\varepsilon)\phi| \\ &\le \varepsilon^3\delta^{2\eta_2}\,\|\gamma\|_{L^4(Y)}\,\|\nabla\bar{u}\|_{L^2(\Omega)}\,\|1-\zeta^\varepsilon\|_{L^\infty(\Omega)}\,\|\phi\|_{L^4(\Omega)} \\ &\le \varepsilon^3\delta^{2\eta_2}\,\|\gamma\|_{H^1(Y)}\,\|\bar{u}\|_{H^1(\Omega)}\,\|1-\zeta^\varepsilon\|_{L^\infty(\Omega)}\,\|\phi\|_{H^1(\Omega)}\,.\end{aligned}$$

Now, using the estimates of $\|\gamma\|_{H^1(Y)}$ and $\|\bar{u}\|_{H^1(\Omega)}$ in (34) and (21), respectively, yields

$$\left|\int_\Omega \Psi_4^\varepsilon \phi\right| \le C\varepsilon^3\delta^{-\eta_1+4\eta_2}\,\|\phi\|_{H^1(\Omega)}\,.$$

Putting the terms together, we obtain

$$\|\Psi^\varepsilon\|_{H^{-1}(\Omega)} \leq C\varepsilon(\varepsilon^2\delta^{-\eta_1+4\eta_2} + \delta^{-\eta_1+3\eta_2}). \tag{17}$$

Using the estimate of $\operatorname{div}(\mathcal{U}^\varepsilon)$ given by (16) and the estimate for $\Psi^\varepsilon$ above, we are able to obtain our final estimate of the residuals. Indeed, from Corollary 6.3 and the residual estimates, we obtain

$$\begin{aligned}\|z_\varepsilon\|_{H(\Omega,\mathrm{div})} &\leq C(\|\Psi^\varepsilon\|_{H^{-1}(\Omega)} + (1+\delta^{\eta_2})\,\|\mathrm{div}(\mathcal{U}^\varepsilon)\|_{L^2(\Omega)})\\ &\leq C(\varepsilon\delta^{-\eta_1+3\eta_2} + \varepsilon^2\delta^{-\eta_1+4\eta_2}),\end{aligned}$$

and from (24), we obtain the pressure estimate

$$\begin{aligned}\|\Xi_\varepsilon\|_{L^2(\Omega)} &\leq C\left((\delta^{\eta_2}+1)\,\|\nabla z_\varepsilon\|_{L^2(\Omega)} + \|\Psi^\varepsilon\|_{H^{-1}(\Omega)}\right)\\ &\leq C(\varepsilon\delta^{-\eta_1+4\eta_2} + \varepsilon^2\delta^{-\eta_1+5\eta_2}).\end{aligned}$$

Thus, the estimate in Theorem 2.1 can be obtained.

**5. Conclusion.** In this paper, we studied the homogenization of high-contrast Brinkman flows and constructed correctors for velocity and pressure under suitable conditions. Under certain assumptions on the coefficients, we proposed the homogenized Brinkman equations and related cell problems. The cell problems were used to compute effective coefficients. For the theoretical analysis, higher-order terms were needed and related cell problems were derived. To correct for the boundary layer, we added a boundary correction term. We presented our main result in Theorem 2.1. This estimate gives us convergence results in some velocity regimes that were discussed in the paper. We presented two numerical test cases: the first is Stokes flow in fractures with Darcy inclusions, and the second is Darcy flow with Stokes flow vuggs. In future work, we wish to extend these results to nonlinear and non-Darcy flows, such as Brinkman–Forcheimer equations. For the case of linear Brinkman equations, the cell problems depend only on the geometry and given Brinkman coefficient $\alpha$. However, in nonlinear flows, the cell solutions cannot be completely decoupled from the macroscale quantities. This fact complicates the homogenization process, and new concepts and tools must be developed.

**6. Appendix: Auxiliary estimates.** Here we present the auxiliary results related to the above results.

**Assumptions on $\alpha, \alpha^*$.** Here we outline the assumptions on $\alpha$ and $\alpha^*$. Throughout we will suppose that $\alpha$ is sufficiently smooth and bounded, satisfying

$$\delta^{\eta_1}\xi\cdot\xi \leq \alpha\xi\cdot\xi \leq \delta^{\eta_2}\xi\cdot\xi, \tag{18a}$$

$$\delta^{\eta_1}\xi\cdot\xi \leq \alpha^*\xi\cdot\xi \leq \delta^{\eta_2}\xi\cdot\xi \tag{18b}$$

for any $\xi\in\mathbb{R}^d$. To guarantee that $\alpha\left(\frac{x}{\varepsilon}\right)$ is high contrast, we suppose that $\eta_2 < 0$.

**Homogenized equation estimates.** Recall the homogenized Brinkman equations (3). Multiplying (3a) by $\bar{u}$ and integrating by parts over $\Omega$, using the divergence free nature of $\bar{u}$, the positivity of $\alpha^*$, and the Cauchy–Schwarz inequality, we observe

$$\begin{aligned}&\int_\Omega |\nabla\bar{u}|^2 + \int_\Omega \alpha^*\bar{u}\cdot\bar{u} = \int_\Omega f\cdot\bar{u}\\ &\leq \left(\int_\Omega |f|^2\right)^{1/2}\left(\int_\Omega |\bar{u}|^2\right)^{1/2} \leq C\left(\int_\Omega |f|^2\right)^{1/2}\left(\int_\Omega |\nabla\bar{u}|^2\right)^{1/2}.\end{aligned}$$

Using the Poincaré inequality we easily obtain

$$\|\bar{u}\|_{H^1(\Omega)} \leq C \|f\|_{L^2(\Omega)}. \tag{19}$$

We assume sufficient smoothness of the domain $\Omega$, forcing $f$, and $\alpha$ for the following. By utilizing the results in [8, 16], we have the follow estimate.

PROPOSITION 6.1. *For $m = 0, 1, 2, \ldots$, assuming sufficient smoothness, we have that if $\bar{u}, \bar{p}$ satisfy* (3)*, then*

$$\|\bar{u}\|_{H^{m+2}(\Omega)} + \|\bar{p}\|_{H^{m+1}(\Omega)} \leq C \|f - \alpha^* \bar{u}\|_{H^m(\Omega)}. \tag{20}$$

*Proof.* See [16] for the proof. ∎

Subsequently, using (18b), (19), and (20), we obtain

$$\|\bar{u}\|_{H^2(\Omega)} \leq C\delta^{\eta_2}\ ,\ \|\bar{u}\|_{H^3(\Omega)} \leq C\delta^{\eta_2}, \tag{21a}$$

$$\|\bar{u}\|_{H^4(\Omega)} \leq C\delta^{2\eta_2}. \tag{21b}$$

**Fine-scale equation estimates.** We will need a priori bounds for the fine-scale equations. Recall that, letting $z_\varepsilon = u_\varepsilon - \mathcal{U}^\varepsilon$ and $\Xi_\varepsilon = p_\varepsilon - \mathcal{P}^\varepsilon$, the fine-scale residual Brinkman equation is of the form

$$\nabla \Xi_\varepsilon - \Delta z_\varepsilon + \alpha\left(\frac{x}{\varepsilon}\right) z_\varepsilon = \Psi^\varepsilon \text{ in } \Omega, \tag{22a}$$

$$\operatorname{div}(z_\varepsilon) = -\operatorname{div}(\mathcal{U}^\varepsilon) \text{ in } \Omega, \quad z_\varepsilon = 0 \text{ on } \partial\Omega, \tag{22b}$$

where $\Psi^\varepsilon = f - \nabla \mathcal{P}^\varepsilon + \Delta \mathcal{U}^\varepsilon - \alpha\left(\frac{x}{\varepsilon}\right)\mathcal{U}^\varepsilon$. For the following estimates we will need the following proposition. Define the spaces $V = \{v : v \in H_0^1(\Omega)^d, \operatorname{div}(v) = 0\}$ and $V^\perp = \{v \in H_0^1(\Omega)^d : (\nabla v, \nabla w) = 0\ \forall\, w \in V\}$.

PROPOSITION 6.2. *The operator* div *is an isomorphism from $V^\perp$ onto $L_0^2(\Omega)$ with*

$$\|\operatorname{div} v\|_{L^2(\Omega)} \geq K \|v\|_{H^1(\Omega)} \quad \text{for all } v \in V^\perp, \tag{23}$$

*where $K$ depends on $d$ and $\Omega$.*

*Proof.* See [8] for the proof. ∎

By Proposition 6.2, there exists $\phi \in V^\perp$ such that

$$\operatorname{div}\phi = \Xi_\varepsilon \text{ in } \Omega,$$
$$\|\Xi_\varepsilon\|_{L^2(\Omega)} \geq K \|\phi\|_{H^1(\Omega)}.$$

From (22), after integration by parts, we have

$$-\int_\Omega \Xi_\varepsilon \operatorname{div}(\phi) + \int_\Omega \nabla z_\varepsilon \nabla \phi + \int_\Omega \alpha\left(\frac{x}{\varepsilon}\right) z_\varepsilon \phi = \int_\Omega \Psi^\varepsilon \phi,$$

and so

$$\begin{aligned}\|\Xi_\varepsilon\|_{L^2(\Omega)}^2 &\leq \left(C(\delta^{\eta_2}+1)\|\nabla z_\varepsilon\|_{L^2(\Omega)} + \|\Psi^\varepsilon\|_{H^{-1}(\Omega)}\right)\|\phi\|_{H^1(\Omega)} \\ &\leq C\left((\delta^{\eta_2}+1)\|\nabla z_\varepsilon\|_{L^2(\Omega)} + \|\Psi^\varepsilon\|_{H^{-1}(\Omega)}\right)\|\Xi_\varepsilon\|_{L^2(\Omega)}.\end{aligned}$$

We arrive at the final pressure estimate

$$\|\Xi_\varepsilon\|_{L^2(\Omega)} \leq C\left((\delta^{\eta_2}+1)\|\nabla z_\varepsilon\|_{L^2(\Omega)} + \|\Psi^\varepsilon\|_{H^{-1}(\Omega)}\right). \tag{24}$$

COROLLARY 6.3. *We have the following estimates:*

$$\begin{aligned}\|\nabla z_\varepsilon\|_{L^2(\Omega)} &\le C(\|\Psi^\varepsilon\|_{H^{-1}(\Omega)} + (1+\delta^{\eta_2})\,\|\mathrm{div}(\mathcal{U}^\varepsilon)\|_{L^2(\Omega)}),\\ \|z_\varepsilon\|_{L^2(\Omega)} &\le C(\|\Psi^\varepsilon\|_{H^{-1}(\Omega)} + (1+\delta^{\eta_2})\,\|\mathrm{div}(\mathcal{U}^\varepsilon)\|_{L^2(\Omega)}),\\ \|z_\varepsilon\|_{H(\Omega,div)} &\le C(\|\Psi^\varepsilon\|_{H^{-1}(\Omega)} + (1+\delta^{\eta_2})\,\|\mathrm{div}(\mathcal{U}^\varepsilon)\|_{L^2(\Omega)}).\end{aligned}$$

*Proof.* Again, from (22), we have

$$\int_\Omega \Xi_\varepsilon \mathrm{div}(\mathcal{U}^\varepsilon) + \int_\Omega |\nabla z_\varepsilon|^2 + \int_\Omega \alpha\left(\frac{x}{\varepsilon}\right)|z_\varepsilon|^2 = \int_\Omega \Psi^\varepsilon z_\varepsilon.$$

Then, since $\alpha$ is positive definite, using the pressure estimate (24) and the Cauchy inequality, we have

$$\begin{aligned}\|\nabla z_\varepsilon\|^2_{L^2(\Omega)} &\le \|\Psi^\varepsilon\|_{H^{-1}(\Omega)}\,\|z_\varepsilon\|_{H^1(\Omega)} + \|\Xi_\varepsilon\|_{L^2(\Omega)}\,\|\mathrm{div}(\mathcal{U}^\varepsilon)\|_{L^2(\Omega)}\\ &\le \|\Psi^\varepsilon\|_{H^{-1}(\Omega)}\,\|z_\varepsilon\|_{H^1(\Omega)}\\ &\quad + C\left((\delta^{\eta_2}+1)\,\|\nabla z_\varepsilon\|_{L^2(\Omega)} + \|\Psi^\varepsilon\|_{H^{-1}(\Omega)}\right)\|\mathrm{div}(\mathcal{U}^\varepsilon)\|_{L^2(\Omega)}\\ &\le C_1\,\|\Psi^\varepsilon\|^2_{H^{-1}(\Omega)} + \frac{1}{4}\,\|\nabla z_\varepsilon\|^2_{L^2(\Omega)} + C_2\,\|\mathrm{div}(\mathcal{U}^\varepsilon)\|^2_{L^2(\Omega)}\\ &\quad + \frac{1}{4}\,\|\nabla z_\varepsilon\|^2_{L^2(\Omega)} + C_3(1+\delta^{\eta_2})^2\,\|\mathrm{div}(\mathcal{U}^\varepsilon)\|^2_{L^2(\Omega)} + \frac{1}{4}\,\|\Psi^\varepsilon\|^2_{H^{-1}(\Omega)}.\end{aligned}$$

Thus,

$$\|\nabla z_\varepsilon\|_{L^2(\Omega)} \le C(\|\Psi^\varepsilon\|_{H^{-1}(\Omega)} + (1+\delta^{\eta_2})\,\|\mathrm{div}(\mathcal{U}^\varepsilon)\|_{L^2(\Omega)}).$$

Using the Poincaré inequality, we obtain the estimate of $\|z_\varepsilon\|_{L^2(\Omega)}$ and, subsequently, the estimate of $\|z_\varepsilon\|_{H(\Omega,\mathrm{div})}$. ∎

**Auxiliary cell equation estimates.** Now that we have estimates for the Brinkman coefficients, the fine scale, and the homogenized equations, we turn to the cell problems (4) and (7). Multiplying (4) by $N$ and integrating, we have

$$\int_Y |\nabla_y N|^2 + \int_Y \varepsilon^2\alpha(y)N : N = \int_Y N : e. \tag{25}$$

From the above equation, using the lower bound of $\alpha$ as in (18a), and standard inequalities, we have

$$\|N\|_{L^2(Y)} \le C\varepsilon^{-2}\delta^{-\eta_1}. \tag{26}$$

To obtain an estimate on the $y$ gradients, we use the general Poincaré inequality and the average relation (5) to yield

$$\begin{aligned}\int_Y |\nabla_y N|^2 &= \int_Y N : e - \int_Y \varepsilon^2\alpha N : N = \int_Y (e - \varepsilon^2\alpha N) : N\\ &= \int_Y (e-\varepsilon^2\alpha N) : (N - \langle N\rangle)\\ &\le \left\|e - \varepsilon^2\alpha N\right\|_{L^2(Y)}\,\|N - \langle N\rangle\|_{L^2(Y)}\\ &\le \left\|e - \varepsilon^2\alpha N\right\|_{L^2(Y)}\,\|\nabla_y N\|_{L^2(Y)}.\end{aligned}$$

Hence, using (26) we have

$$\|\nabla_y N\|_{L^2(Y)} \leq \left\|e - \varepsilon^2 \alpha N\right\|_{L^2(Y)} \leq C\delta^{-\eta_1+\eta_2}. \tag{27}$$

Subsequently, by Proposition 6.2, we have

$$\|Q\|_{L^2(Y)} \leq C\delta^{-\eta_1+\eta_2}. \tag{28}$$

Furthermore, we will need estimates for the next-order cell solutions $\gamma$ given by (7). We will follow the presentation in [17]. First, define the spaces $L^2_{\#}(Y) = L^2_{sol,\#}(Y) \bigoplus V^2_{pot,\#}(Y)$, where $L^2_{\#}(Y) = \{u \in L^2(Y),\ u\ y\text{-periodic}\}$; similarly, we can define $H^1_{\#}(Y)$. In addition, define $V^2_{pot,\#}(Y) = \{\nabla u,\ u \in H^1_{\#}(Y)\}$ and $L^2_{sol,\#}(Y) = \{u \in L^2_{\#}(Y),\ \mathrm{div}(u) = 0\}$.

Thus, $\gamma$ can be decomposed as $\gamma = \gamma_1 + \gamma_2$ with $\gamma_1 \in V^2_{pot,\#}(Y)$ and $\gamma_2 \in L^2_{sol,\#}(Y)$; i.e., there exists $u \in H^1_{\#}(Y)$ such that $\gamma_1 = \nabla u$ and $\mathrm{div}(\gamma_2) = 0$. Using the cell equation (7), we deduce that

$$\Delta u = -N + \varepsilon^{-2}|Y|^{-1}(\alpha^*)^{-1} \text{ in } Y, \tag{29}$$

with $u$ being $y$-periodic. Thus,

$$\mathrm{div}(\gamma_2) = 0 \text{ in } Y, \tag{30}$$

with $\gamma_2$ being $y$-periodic and $\langle \gamma_2 \rangle_Y = 0$. We observe that $\gamma_2 = 0$ satisfies (30), and thus we can select

$$\gamma = \nabla u. \tag{31}$$

Since $\left\langle -N(y) + \varepsilon^{-2}|Y|^{-1}(\alpha^*)^{-1} \right\rangle_Y = 0$, by the Lax–Milgram theorem, (29) has a unique solution. Thus, we easily obtain get the following estimate:

$$\|\nabla u\|_{L^2(Y)} \leq \|\nabla N\|_{L^2(Y)}. \tag{32}$$

Now we calculate $\|\nabla\gamma\|_{L^2(Y)}$. Taking $\frac{\partial}{\partial y_j}$ of (29), for $j = 1, 2, \ldots, d$, yields

$$\Delta \frac{\partial}{\partial y_j} u(y) = -\frac{\partial}{\partial y_j} N(y) \text{ in } Y,$$

along with periodic boundary conditions. We arrive at the following estimate:

$$\left\|\nabla^2 u\right\|_{L^2(Y)} \leq C \|\nabla N\|_{L^2(Y)}. \tag{33}$$

Therefore, by (27), (31), (32), and (33), we obtain

$$\|\gamma\|_{L^2(Y)} \leq C\delta^{-\eta_1+\eta_2}, \tag{34a}$$

$$\|\mathrm{div}(\gamma)\|_{L^2(Y)} \leq C\delta^{-\eta_1+\eta_2}, \tag{34b}$$

$$\|\nabla\gamma\|_{L^2(Y)} \leq C\delta^{-\eta_1+\eta_2}. \tag{34c}$$

**Sobolev embedding theorems.** We have used the Sobolev embedding theorem and a generalized Holder inequality repeatedly throughout this paper. They can be found in [6, 7], and we now list the theorems briefly here for completeness.

THEOREM 6.4. *Suppose that* $1 \le p_j \le \infty$ *and* $\sum_1^n p_j^{-1} = r^{-1} \le 1$. *If* $f_j \in L^{p_j}$, *for* $j = 1, \dots, n$, *then* $\Pi_1^n f_j \in L^r$ *and* $\|\Pi_1^n f_j\|_r \le \Pi_1^n \|f_j\|_{p_j}$.

THEOREM 6.5. *If* $\Omega$ *is a compact domain with smooth boundary in* $\mathbb{R}^n$, *then there is a constant* $C = C(\Omega)$ *such that*

$$\|f\|_{W^{m-k,q}(\Omega)} \le C \|f\|_{W^{m,p}(\Omega)} \quad \text{for all } f \in W^{m,p}(\Omega), \tag{35}$$

*where* $\frac{k}{n} < \frac{1}{p} \le 1$, $\frac{1}{q} \ge \frac{1}{p} - \frac{k}{n}$.

THEOREM 6.6. *If* $\Omega$ *is a compact domain with smooth boundary in* $\mathbb{R}^n$, *then there is a constant* $C = C(\Omega)$ *such that*

$$\|f\|_{W^{m-k,q}(\Omega)} \le C \|f\|_{W^{m,p}(\Omega)} \quad \text{for all } f \in W^{m,p}(\Omega), \tag{36}$$

*where* $\frac{k}{n} = \frac{1}{p}$, $q < \infty$.

By Theorems 6.4 and 6.6 we obtain

$$\|fg\|_{L^2(\Omega)} \le \|f\|_{L^4(\Omega)} \|g\|_{L^4(\Omega)} \tag{37}$$

$$\le \|f\|_{H^1(\Omega)} \|g\|_{H^1(\Omega)}, \tag{38}$$

provided that $f$, $g \in H^1(\Omega)$ for $n = 2$, 3 and for sufficiently smooth domains.

**Acknowledgment.** The authors would like to thank Dr. Juan Galvis for his codes for the Stokes equation and his great patience in helping us implement our problems.

## REFERENCES

[1] G. ALLAIRE, *Homogenization and two-scale convergence*, SIAM J. Math. Anal., 23 (1992), pp. 1482–1518.

[2] T. ARBOGAST AND H. L. LEHR, *Homogenization of a Darcy-Stokes system modeling vuggy porous media*, Comput. Geosci., 10 (2006), pp. 291–302.

[3] D. L. BROWN, P. POPOV, AND Y. EFENDIEV, *On homogenization of Stokes flow in slowly varying media with applications to fluid-structure interaction*, GEM Int. J. Geomath., 2 (2011), pp. 281–305.

[4] G. A. CHECHKIN, A. L. PIATNISKI, AND A. S. SHAMEV, *Homogenization: Methods and Applications*, Transl. Math. Monogr. 234, American Mathematical Society, Providence, RI, 2007.

[5] H. DARCY, *Les fontaines publique de la ville de Dijon*, Librairie des Corps Impériaux des Ponts et Chaussées et des Mines, Paris, 1856.

[6] L. C. EVANS, *Partial Differential Equations*, American Mathematical Society, Providence, RI, 1998.

[7] G. B. FOLLAND, *Real Analysis: Modern Techniques and Their Applications*, John Wiley & Sons, New York, 1999.

[8] V. GIRAULT AND P. A. RAVIART, *Finite Element Methods for Navier-Stokes Equations*, Springer-Verlag, Berlin, 1986.

[9] O. ILIEV, R. LAZAROV, AND J. WILLEMS, *Variational multiscale finite element method for flows in highly porous media*, Multiscale Model. Simul., 9 (2011), pp. 1350–1372.

[10] E. MARUSIC-PALOKA AND A. MIKELIC, *An error estimate for correctors in the homogenization of the Stokes and Navier-Stokes equations in a porous medium*, Boll. Un. Mat. Ital. A (7), 10 (1996), pp. 661–671.

[11] O. A. OLEINIK, G. A. IOSIF'YAN, AND A. S. SHAMAEV, *Mathematical Problems in Elasticity and Homogenization*, Elsevier, Amsterdam, 1992.

[12] P. Popov, G. Qin, L. Bi, Y. Efendiev, R. Ewing, Z. Kang, and J. Li, *Multiscale methods for modeling fluid flow through naturally fractured carbonate karst reservoirs*, in Proceedings of the SPE Annual Technical Conference and Exhibition, SPE 110778, 2007.
[13] E. Sanchez-Palencia, *Non-homogeneous Media and Vibration Theory*, Lecture Notes in Phys. 127, Springer-Verlag, Berlin, 1980.
[14] E. Sanchez-Palencia and H. I. Ene, *Equations et phénomènes de surface pour l'écoulement dans un modèle de milieu poreux*, J. Mécanique, 14 (1975), pp. 73–108.
[15] L. Tartar, *Incompressible fluid flow in a porous medium: Convergence of the homogenization process*, in Non-homogeneous Media and Vibration Theory, Lecture Notes in Phys. 127, Springer-Verlag, Berlin, 1980, pp. 368–377.
[16] R. Temam, *Navier-Stokes Equations: Theory and Numerical Analysis*, North–Holland, Amsterdam, New York, Oxford, 1977.
[17] V. V. Zhikov, S. M. Kozlov, and O. A. Oleinik, *Homogenization of Differential Operators and Integral Functionals*, Springer-Verlag, Berlin, 1994.